Simple hydrothermal synthesis method for tailoring the physicochemical properties of ZnO: morphology…

1 author:

Simple hydrothermal synthesis method for tailoring the physicochemical properties of ZnO: morphology, surface area and polarity

Hugo Silva,[a] Cecilia Mateos-Pedrero,*[a] Cesar Magén,[b] David A. Pacheco Tanaka†[a] and Adélio Mendes*[a]

A simple urea-assisted hydrothermal synthesis method was used to tailor the physicochemical properties of ZnO materials. The role of Pluronic P123 block copolymer in the crystal growth, morphology and specific surface area of the as-prepared ZnO was studied. When Pluronic P123 is used, well-dispersed hierarchical microspheres, with a flower-like morphology, are obtained, but in its absence large spherical agglomerated clusters are formed. The polarity of the ZnO, measured as the ratio between plane (002) and plane (100), is also significantly higher for the Pluronic P123 sample. The influence of zinc salt precursors was also analysed. The use of zinc nitrate led to the formation of urchin-like ZnO structures, instead of the microflowers that result from zinc acetate salt. Despite having similar surface areas, the polarity of the zinc nitrate sample was much smaller. The decomposition of methylene blue corroborated the higher photocatalytic activity of the ZnO materials with a higher proportion of polar planes (higher polarity). The formation mechanism of the crystals is also suggested based on the observed gradual growth and assembly of the hydrozincite during the initial steps of the synthesis for the samples with and without Pluronic P123.

Introduction

ZnO is a semiconductor material that has attracted research interest during the last few years, mainly focusing on application-related aspects.[1–3] Among the wide range of multifunctional applications it is possible to highlight the following high-technology uses: emitting diodes,[4] piezoelectric transducers,[5] lasers,[6] hydrogen sensors,[5] biosensors[6] and inorganic antimicrobial agents.[7] Tailoring the main properties of such a versatile material towards a performance enhancement is of critical importance. Presently, looking inside the catalysis field, including photocatalysis, there is a continuous search of ZnO nanostructures that contain high surface areas and a large number of surface defects. These key properties have proved to be valuable in methanol reactions, such as methanol steam reforming and methanol synthesis,[8–11] and in photocatalysis where ZnO is pointed to be a suitable alternative of TiO$_2$.[12,13] ZnO has a wurtzite crystalline structure with unbalanced

charges either terminated in Zn^{2+} or O^{2-}, corresponding, respectively to Zn–ZnO(0001) and O–ZnO(000−1) polar planes.[14,15] The basal polar planes of ZnO were reported to be much more active in photocatalysis as compared to the non-polar facets, due to a higher density of defects such as oxygen vacancies.[16] Plane-density functional theory calculations performed by Guo *et al.* also indicate the contribution of polar facets for a low-temperature pathway reaction of methanol steam reforming;[17] according to their calculations the dissociation of both water and methanol have low or null barriers on the polar Zn–ZnO(0001). The effect of different nanoshapes of ZnO in methanol steam reforming and water gas-shift reactions was studied by Flytzani-Stephanopoulos *et al.* and the activity was higher with the increasing number of polar facets exposed.[18] According to the former studies, it is easy to understand that a large surface area (0001) ZnO is beneficial from the catalysis point of view.

Different synthesis methods for preparing highly faceted nanostructures, which expose mainly polar planes, were investigated. For instance, Li *et al.*, prepared ZnO with various morphologies using a hydrothermal route.[19] The morphology of the ZnO hexagonal planes presented a high proportion of polar planes and nevertheless the surface area was very low: 4.6 m^2 g^{-1}. A similar hexagonal plate-like morphology was produced by Mclaren *et al.* using a chemical synthetic route and oleic acid as capping agent, proving to be very effective towards the decomposition of methylene blue.[20] However, in the former study

[a]*LEPABE-Departamento de Engenharia Química, Faculdade de Engenharia da Universidade do Porto, Rua Dr Roberto Frias, 4200-465 Porto, Portugal. E-mail: cmpedrero@fe.up.pt; amendes@fe.up.pt*

[b]*Laboratorio de Microscopías Avanzadas (LMA), Instituto de Nanociencia de Aragón INA-ARAID, Departamento de Física de la Materia Condensada, Universidad de Zaragoza, 50018 Zaragoza, Spain*

† Presently at Tecnalia, Parque Tecnológico de San Sebastián Paseo Mikeletegi, 2. 20009 Donostia, San Sebastián, Spain.

there is no mention to the surface area of ZnO. A non-hydrolytic aminolysis synthesis route was used for the preparation of nanocones with predominant [0001] polar planes but again the surface area was as low as 17.3 m^2 g^{-1}.[21] Burton et al. investigated routes for obtaining a high surface area ZnO material with increased proportion of polar planes using a sodium citrate; these authors used a capping agent for blocking the growth along the [0001] direction.[22] Unfortunately, despite had achieving a highly faceted morphology, the surface area dropped from 96 m^2 g^{-1} to 48 m^2 g^{-1} when the calcination temperature was raised from 120 °C to 340 °C, respectively; this former temperature corresponded to ZnO without traces of reactant intermediates. Therefore, it was concluded that the developed ZnO did not present the desired thermal stability.

Thermally stable 3D microflowers of ZnO with a high surface area and proportion of polar planes were prepared in this work. The photocatalytic performance of the optimized materials was successfully tested in the decomposition of blue methylene. The hydrothermal method was followed due to its simplicity, low cost, high yields, easy scaling up, facile control over nanocrystal growth and mild conditions requirements.[23] It is known that the growth velocities (V) of the crystal planes follow this preferential order: $V(0001) > V(10\bar{1}1) > V(10\bar{1}0)$ due to the differences in surface energy between the planes.[24,25] However, the slow hydrolyses of urea and the presence of block copolymer P123 as template agent inhibited the growth in the (0001) direction. The obtained ZnO materials were characterized by N_2 physisorption, electron energy disperse spectroscopy (EDS) in combination with scanning electron microscopy (SEM), high resolution transmission electron microscopy (HR-TEM) with selective area electron diffraction (SAED), X-ray powder diffraction (XRD), differential scanning calorimetry-thermal gravimetric analysis (DSC-TGA) and X-ray photoelectron spectroscopy (XPS).

Experimental

Synthesis of ZnO samples

Zinc acetate dihydrate ($Zn(CH_3COO)_2 \cdot 2H_2O$; 99.0%), zinc nitrate hexahydrate ($Zn(NO_3)_2 \cdot 6H_2O$; 98.0%), urea ($CO(NH_2)_2$; 99.5%), glacial acetic acid (CH_3COOH; 99.7%), block copolymer poly(ethylene glycol)-block-poly(propylene glycol)-block-poly-(ethylene glycol) (Pluronic P123, PEG20-PPG70-PEG20), were obtained from Sigma-Aldrich and used without further purification. Distilled water was used throughout the experiments. In a typical synthesis the ZnO support precipitate was obtained as following: 5 mmol of zinc salt precursor (acetate or nitrate, Table 1), 100 mmol of urea and given amounts of Pluronic P123 (Table 1) were mixed in 100 mL of distilled water. The pH of the solution was adjusted to 5.0 with glacial acetic acid and stirred for 2 h under ambient conditions. Then the mixture was poured into a 150 mL Teflon-lined autoclave and maintained at a given temperature (Table 1) for 24 h and cooled down to room temperature naturally. The white precipitate was thoroughly washed with distillated water and dried overnight at 110 °C. The final ZnO powder was obtained after calcination in a muffle furnace at a given temperature (Table 1) for 30 minutes.

Characterization

The specific surface area (S_{BET}) of the ZnO materials was determined by standard N_2 gas adsorption method using a Quantachrome Autosorb-1 apparatus. XRD measurements were taken on a Rigaku Miniflex 2. SEM analysis was performed using a FEI Quanta 400 scanning electron microscope equipped with an energy dispersive X-ray high vacuum detector (EDX). HR-TEM/SAED images were obtained using a FEI Titan High Base microscope. DSC-TGA analyses were performed using a Netzsch TG 209 F1 Iris instrument. The photocatalytic activity of selected ZnO samples was assessed based on the decomposition of methylene blue (MB solution: 0.01 g L^{-1}). During the experiments, 100 mL of solution was poured into a glass flask with 50 mg of ZnO. A UV lamp (Vilber Lourmat, BLB 365 nm, 2 × 6 W) was placed over the solution and maintained at the same distance during the experimental tests (irradiance of 10 W m^{-2}). The extent of MB degradation was determined measuring the absorbance of the solution at 645 nm. XPS analyses were performed using a Kratos AXIS Ultra HSA, with VISION software for data acquisition and CASA XPS software for data analysis. The analysis was carried out with a monochromatic Al Kα X-ray source (1486.7 eV), operating at 15 kV. For the quantification of the elements, sensibility factors provided by the manufacturers were used. For these experiments, Zn 2p, O 1s and C 1s bands were recorded. The binding energies were calibrated by fixing the C–(C, H) contribution of the C 1s adventitious carbon at 285.0 eV.

Results and discussion

Characterization of the ZnO precursor: the role of Pluronic P123

The thermal decomposition of the ZnO precursor (before calcination) for the samples prepared in the absence ($Zn_{Ac}P0T90$) and presence of Pluronic P123 ($Zn_{Ac}P10T90$, Table 1) was examined by TG-DSC.

The following nomenclature for the prepared ZnO samples was used (Table 1), Zn_xPyTz, where: x denotes the zinc precursor, zinc-acetate (Ac) or zinc-nitrate (N); Py stands for the amount of Pluronic P123 expressed as (n_{P123}/n_{Ac}) molar ratio percentage (Table 1) and Tz represents the synthesis temperature in °C (Table 1). Accordingly, the $Zn_{Ac}P10T90$ sample was prepared from zinc-acetate as precursor, with a (n_{P123}/n_{Ac}) molar ratio% of 10 and at 90 °C.

The TG-DSC results obtained for sample $Zn_{Ac}P10T90$ are shown in Fig. 1A. As depicted in this figure, this sample was decomposed in only one fast step, denoted by a sharp peak centered at 250 °C. This was accompanied by a weight loss of 26% in the temperature interval of 175–300 °C. The sample prepared without P123 behave similarly (results not shown here). In fact both samples exhibit the same TG profile, indicating that Pluronic P123 was removed during the washing step.

The evolution of the CO_2 during the thermal decomposition of $Zn_{Ac}P10T90$ sample was followed by mass spectroscopy. As shown in Fig. 1B, a large CO_2 peak is observed centered at 250 °C, in agreement with TG-DSC data. The decomposition

Table 1 Experimental parameters studied for the preparation of ZnO samples (Zn_xPyTz: x Zn-precursor; Py Pluronic P123 amount; Tz synthesis temperature)

Parameter studied	Range	Sample name
ZnO-precursor	Zn-acetate	$Zn_{Ac}P10T90$
	Zn-nitrate	$Zn_NP10T90$
P123 concentration (n_{P123}/n_{Ac}) molar ratio%	0	$Zn_{Ac}P0T90$
	3	$Zn_{Ac}P3T90$
	7	$Zn_{Ac}P7T90$
	10	$Zn_{Ac}P10T90$
	20	$Zn_{Ac}P20T90$
Synthesis temperature (°C)	70	$Zn_{Ac}P10T70$
	90	$Zn_{Ac}P10T90$
	110	$Zn_{Ac}P10T110$
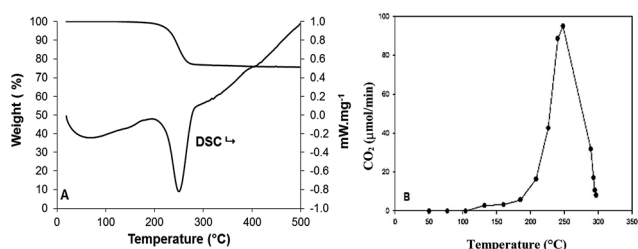
Fig. 1 (A) TGA-DSC analyses of the ZnO-precursor (before calcination) at a heating rate of 10° min^{-1} in static air for $Zn_{Ac}P10T90$ sample; (B) thermal decomposition of the ZnO-precursor followed by mass spectroscopy.

value for the zinc hydroxycarbonate (hydrozincite) according to eqn (1) is 26.3 wt%, which is in good agreement with the TG results (26%).

$$Zn_5(CO_3)_2(OH)_6 \rightarrow 5ZnO + 3H_2O + 2CO_2 \tag{1}$$
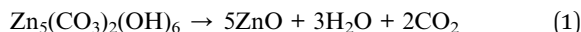
On the other hand, according to the XRD pattern of both samples (not shown), all the diffraction peaks could be indexed as hydrozincite (hereafter referred to as HZC, Fig. 4), $Zn_5(CO_3)_2(OH)_6$, (JCPDS Card no. 19-1458).

The effect of Pluronic P123 on the morphology of the as-prepared HZC samples (before calcination) is nicely illustrated in Fig. 2. In the absence of additive, spherical clusters of HZC appear to be agglomerated forming larger clusters of about 200 μm (Fig. 2A). The addition of Pluronic P123 resulted in well-dispersed microspheres (Fig. 2B), which are in fact microflower-like in morphology (inset Fig. 2B).

Comparing images in Fig. 2, it is clear that spherical HZC architectures are obtained, regardless of Pluronic P123 content, being the main difference the higher dispersion of these microspheres in the presence of Pluronic P123. The calcination effect on the structure and morphology of the resulting ZnO solids (from HZC prepared in the absence and presence of Pluronic P123) was analyzed by XRD and SEM.

It is important to mention that repetition of the synthesis under identical conditions led to similar results. SEM micrographs in Fig. 3 reveal very different morphologies for both samples. In the absence of Pluronic P123 (Fig. 3A) non

homogeneous ZnO structures ($Zn_{Ac}P0T90$), consisting of a combination of plates and spheres, were formed. The enlarged SEM image of one single sphere in Fig. 3B–C, shows that it is composed of randomly close-packed porous nanosheets.

On the contrary, in the presence of Pluronic P123 (sample $Zn_{Ac}P10T90$) well-dispersed ZnO microspheres were obtained (Fig. 3D). Moreover, SEM images in Fig. 3D and E clearly show that the ZnO product calcined at 375 °C inherited the flower-like morphology of the HZC precursor (Fig. 3B), evidencing its thermal stability.

According to Fig. 3D–F, calcination of HZC resulted in ZnO samples (sample $Zn_{Ac}P10T90$) made up of micro-flowers
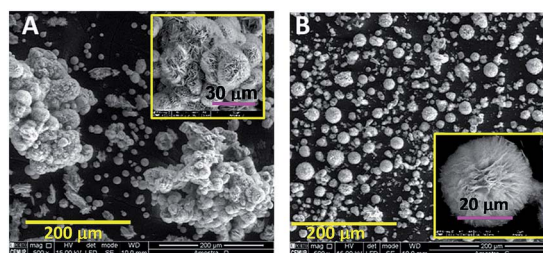
Fig. 2 SEM images of the as-prepared HZC samples obtained in the absence (A) and presence of Pluronic P123 (B) (n_{P123}/n_{Ac} molar ratio = 0.10).
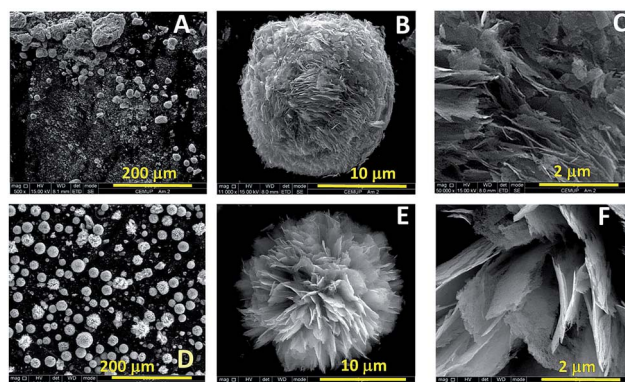
Fig. 3 Low and high magnification SEM images of ZnO samples $Zn_{Ac}P0T90$ (A–C) and $Zn_{Ac}P10T90$ (D–F).

uniformly distributed and of smaller diameter (21 μm) than those seen in the HZC precursor (35 μm) (Fig. 2B). Detailed observation of a single micro-flower in Fig. 3E shows that they are in fact an assembly of nanosheets that grow radially from the center outward, and the entire structure resembles a carnation. The micro-flowers in $Zn_{Ac}P10T90$ sample show a lot of voids between the various nanosheets (Fig. 3E and F), in opposition to the compact structure shown by the $Zn_{Ac}P0T90$ sample (prepared without Pluronic P123; Fig. 3B and C). This is also reflected in the high specific surface area that is 43% larger for sample $Zn_{Ac}P10T90$ (80 m^2 g^{-1}) than that of the sample $Zn_{Ac}P0T90$ (46 m^2 g^{-1}). Thus, the presence of Pluronic P123 helps to enhance the formation of spherical ZHC structures during the hydrothermal synthesis. As a result the ZnO product obtained after calcination, inherits the flower-like morphology of the ZHC precursor maintaining also the high dispersion.

The XRD patterns of $Zn_{Ac}P0T90$ and $Zn_{Ac}P10T90$ samples are shown in Fig. 4 with an SAED image of each nanostructure in the inset.

It is found that both samples are highly crystalline, and the diffraction peaks in every pattern can be indexed to hexagonal wurtzite-type ZnO (JCPDS no. 36-1451). No other phases were detected indicating pure ZnO samples. Further EDX results confirmed that the ZnO samples were composed of solely Zn and O. However, the diffraction intensity ratios of (002) polar plane to (100) nonpolar plane are clearly different from one sample to another. In the present work, the term "polarity" is used to refer the relative intensities ratio of the polar and the nonpolar planes, ($I_{(002)}/I_{(100)}$). In this way, intensity ratio values higher than the wurtzite reference ($I_{(002)}/I_{(100)} = 0.73$) denote a higher polarity, and consequently a higher ratio of exposed polar facets, and *vice versa*. The polarity values ($I_{(002)}/I_{(100)}$) for samples $Zn_{Ac}P0T90$ and $Zn_{Ac}P10T90$ are 0.74 and 1.10,
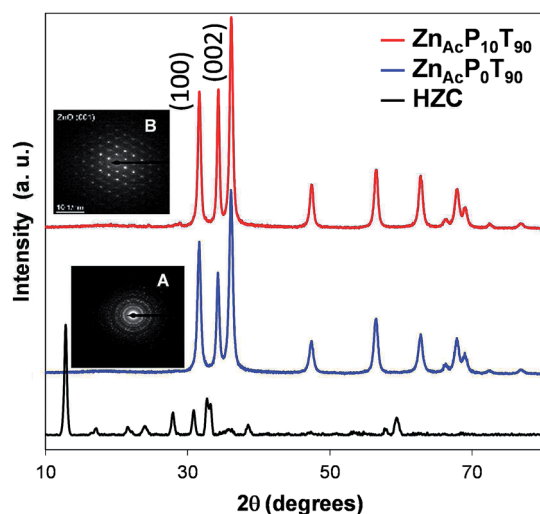
respectively. Clearly, the former sample shows the same polarity as the reference wurtzite, whereas the latter has a higher polarity. This indicates that the use of Pluronic P123 enhances the polarity of the ZnO material.

SAED patterns were also obtained for samples $Zn_{Ac}P0T90$ and $Zn_{Ac}P10T90$ (insets A and B in Fig. 4). The $Zn_{Ac}P0T90$ sample shows a diffraction pattern characteristic of a fully polycrystalline material with preferential growth along the *c*-axis direction (inset A in Fig. 4). On the other hand, the SAED pattern of the $Zn_{Ac}P10T90$ sample confirms that they are single crystals (inset B in Fig. 4).

These results demonstrate that the addition of Pluronic P123 strongly influences the morphology and the growth preference of ZnO materials prepared by the hydrothermal route. In particular, in the presence of Pluronic P123 hierarchical ZnO microflowers whose surface is dominated by their (002) polar planes were formed.

The influence of the ZnO precursor

Since the most promising ZnO material was obtained in the presence of Pluronic P123 ($Zn_{Ac}P10T90$), we focused on the optimization of its preparation. Accordingly, a series of ZnO samples were prepared following the same procedure as for the $Zn_{Ac}P10T90$ sample by only changing one parameter while keeping the rest to be constant. The following parameters were studied: ZnO precursor, Pluronic P123 concentration and hydrothermal synthesis temperature (Table 1). The influence of these parameters on the specific surface area, morphology, structure and growth habit (polarity) of ZnO products is discussed in next sections.

The influence of the Zn-precursor on the morphology of the prepared ZnOs is presented in Fig. 5.

The use of zinc nitrate ($Zn_NP10T90$) resulted in the formation of sea urchin-like ZnO structures (Fig. 5A) made of very thin ZnO nanowires (*ca.* 25 nm thick; Fig. 5B). As previously indicated, the sample synthesized from zinc acetate ($Zn_{Ac}P10T90$) presents a lamellar flower-like architecture (Fig. 5C and D),

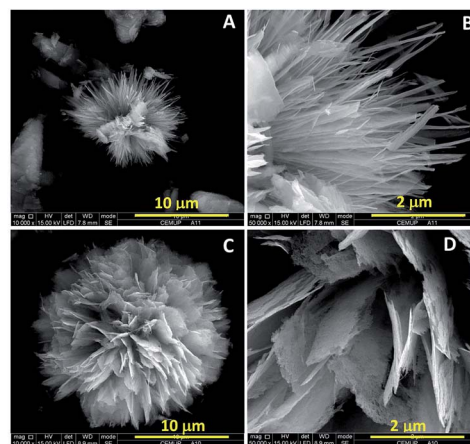**Fig. 4** XRD pattern of $Zn_5(CO_3)_2(OH)_6$ precursor (HZC) and ZnO samples prepared in the absence ($Zn_{Ac}P0T90$) and presence of Pluronic P123 ($Zn_{Ac}P10T90$) after calcination at 375 °C for 30 minutes. Inset (A): SAED pattern of $Zn_{Ac}P0T90$ sample. Inset (B): SAED pattern of $Zn_{Ac}P10T90$ sample.

Fig. 5 SEM images of ZnO samples prepared with different types of metal salts: zinc nitrate, $Zn_NP10T90$, (A and B) and zinc acetate, $Zn_{Ac}P10T90$, (C and D).

made up of assembled porous ZnO nanosheets (*ca.* 23 nm thick). Considering the size of these ZnO materials, it is found that the Zn-nitrate precursor leads to smaller ZnO structures (mean size 12 µm; Fig. 5A) in comparison with its Zn-acetate counterpart (mean size 20 µm; Fig. 5B).

Both samples have a quite similar specific surface area (80 and 76 m^2·g^{-1} for Zn$_{Ac}$P10T90 and Zn$_N$P10T90 samples, respectively), and also show the same wurtzite structure although the relative intensities of the polar (100) and nonpolar (002) XRD planes are very different. The latter suggests that the growth habit of ZnO crystals is different in both samples. As already mentioned, the Zn$_{Ac}$P10T90 sample has a higher polarity ($I_{(002)}/I_{(100)} = 1.10$) than the reference wurtzite. In contrast, the Zn$_N$P10T90 sample (prepared from zinc nitrate) shows lower polarity ($I_{(002)}/I_{(100)} = 0.60$). This indicates that the zinc salt precursor influences the growth habit of the resulting ZnO products. This might be related to the different morphologies of both ZnO products as reported in.[26–28] In the case of Zn$_{Ac}$P10T90 sample the flowers are composed of plates (Fig. 5D); this kind of structures are likely originated from lateral growth along the nonpolar facets of ZnO then explaining their increased polarity in a similar fashion as described in.[20,22,29,30] On the other hand, the urchin structures formed in Zn$_N$P10T90 are made up of needles (Fig. 5B). According to the literature[31–33] the usual growth along *c*-axis is expected to occur in such a case, explaining the lower polarity of the Zn$_N$P10T90 sample.

The influence and role of the Pluronic P123 concentration

The SEM images of the samples prepared with increasing Pluronic P123 concentration (Table 1) are depicted in Fig. 6. The sample prepared with the lowest Pluronic P123 amount (Zn$_{Ac}$P3T90; n_{P123}/n_{Ac} molar ratio = 0.03) consists of ZnO particles of irregular shapes (Fig. 6A). The morphology of Zn$_{Ac}$P7T90 and Zn$_{Ac}$P10T90 samples (n_{P123}/n_{Ac} molar ratio = 0.07 and 0.10, respectively; Table 1) is similar. In fact, both samples have a flower-like morphology (mean size of about 20 µm) assembled from ZnO plates (Fig. 6B and C), although Zn$_{Ac}$P10T90 has a higher number of voids between the sheets (compare inset in Fig. 6B and C). The structure became more compact as the P123 concentration increases (Fig. 6D), resulting in the formation of non-uniform agglomerated particles, where no ZnO nanoplates are apparent (inset Fig. 6D), as for the Zn$_{Ac}$P20T90 sample (n_{P123}/n_{Ac} molar ratio = 0.20).

The evolution of the specific surface area with the Pluronic P123 content (Fig. 7) also points to the same conclusions. As shown in Fig. 7 the surface area steadily increases with the Pluronic P123 content until an optimum value (0.10 molar ratio, Zn$_{Ac}$P10T90, $S_{BET} = 80$ m^2 g^{-1}). Further increase causes to significantly decrease the surface area, in good agreement with the agglomeration of this sample as suggested by SEM.

In all cases the final ZnO solids displayed XRD patterns characteristic for wurtzite (Fig. 8). As observed in Fig. 8, significant changes in the relative intensities of the polar (002) and nonpolar (100) planes are observed with varying the Pluronic P123 content.

The sample with the lowest Pluronic P123 content (Zn$_{Ac}$P3T90) has essentially the same polarity (Fig. 8) as the wurtzite reference ($I_{(002)}/I_{(100)} = 0.76$ and 0.73 for Zn$_{Ac}$P3T90 and wurtzite, respectively), indicating that this sample follows the growth habit of ZnO crystals along *c*-axis.

As the P123 molar ratio was increased (Zn$_{Ac}$P7T90 and Zn$_{Ac}$P10T90 samples) substantial growth of the polar (002) plane is found (Fig. 8). Both samples have higher polarity than the wurtzite ($I_{(002)}/I_{(100)} = 0.94$ and 1.10 for Zn$_{Ac}$P7T90 and Zn$_{Ac}$P10T90, respectively). In contrast, further increase of P123 content, (Zn$_{Ac}$P20T90) resulted in the opposite effect. Therefore, for Zn$_{Ac}$P20T90 sample the nonpolar (100) peak has a higher intensity than that of the wurtzite, indicating a lower polarity, namely, a lower ratio of exposed polar facets.

Additionally, the microspheres are almost absent from the Zn$_{Ac}$P20T90 sample, which is mainly constituted by nanoflakes without a clear and well-defined morphology. Peng Bai *et al.*, had a similar result when the concentration of Pluronic was increased to an extreme value. This phenomena was attributed to an excess of surfactant in solution leading to high viscosities
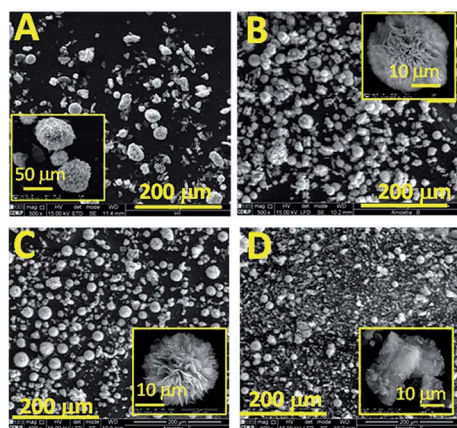

Fig. 6 SEM images of the ZnO products prepared with different n_{P123}/n_{Ac} molar ratios: (A) 0.03 (Zn$_{Ac}$P3T90), (B) 0.07 (Zn$_{Ac}$P7T90), (C) 0.10 (Zn$_{Ac}$P10T90), (D) 0.20 (Zn$_{Ac}$P20T90).

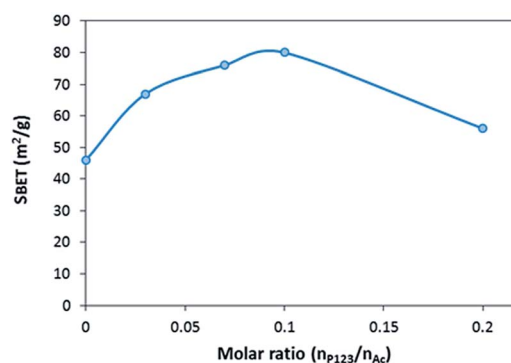**Fig. 7** Evolution of the specific surface area of ZnO samples as a function of the Pluronic P123 content (Zn$_{Ac}$PyT90 series: Zn-acetate and hydrothermal temperature 90 °C). Lines were added for readability.
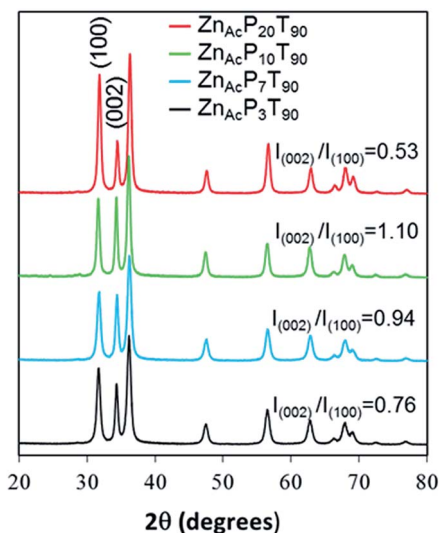
Fig. 8 XRD pattern and $I_{(002)}/I_{(100)}$ ratio of the ZnO samples synthesized from Zn-acetate, at 90 °C and with different Pluronic P123 content.

that can reduce the mobility of nanoparticles and hinder the self-assembly process.[34]

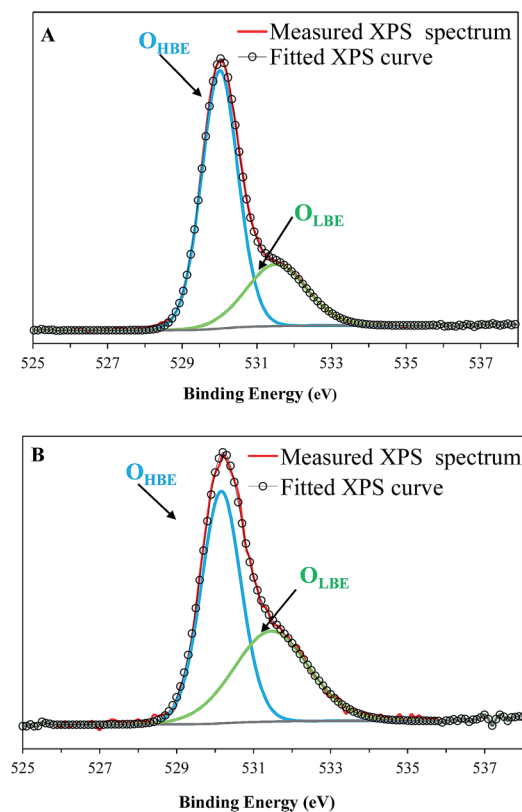The surface of this series of samples was characterized by XPS (Fig. 9). All samples show Zn and O as main elements (being the atomic ratio about 1, as expected for ZnO) along with trace amount of adventitious carbon contaminant. For all the samples, the Zn 2p$_{3/2}$ XPS spectrum is centered at 1021.3 $\pm$ 0.2 eV with a symmetrical peak type, indicating that it exists only in the oxidized state Zn^{2+}.[35] On the other hand, the O 1s photo-electron peak is asymmetrical and presents a visible shoulder on the high binding energy side (Fig. 9). The O 1s XPS peak can be fitted using two Gaussian components centered at 530.1 eV (low binding energy oxygen, referred as O_{LBE}) and 531.5 eV (high binding energy oxygen, referred as O_{HBE}), respectively. According to the literature the first component 530.1 eV (O_{LBE}) is attributed to O^{2-} ions on wurtzite structure of hexagonal Zn^{2+} ion array, surrounded by Zn atoms with their full complement of nearest-neighbour O^{2-} ions. The O_{HBE} is associated with O^{2-} in oxygen deficient regions within the matrix of ZnO.

As clearly visible in Fig. 9 and Table 2, the relative ratio of both components is different for the various samples. In fact, the relative ratio of the O_{HBE} component appears to increase with P123 amount between 0.03 and 0.10 molar ratio, indicating that increasing the amount of P123 within this ratio contributes to enhance the number of oxygen defects, in good agreement with the above conclusions. The surface composition of the ZnO samples, based on XPS spectra, revealed that the concentration of oxygen vacancies tend to increase with the P123 concentration.

It is clear that the P123 content strongly influences the morphology, the specific surface area, the surface composition and the growth habit of ZnO samples. Our results evidence that there is an optimum range that allows preparing homogeneous hierarchical ZnO structures with enhanced specific surface area and polarity. All these properties make this kind of ZnO materials good candidates for a wide range of applications such as: catalysis,[8–11] emitting diodes,[4] piezoelectric transducers,[5] lasers,[6] hydrogen sensors,[5] biosensors[6] and inorganic antimicrobial agents.[7]

The role of Pluronic P123 on the morphology of ZnO

Due to their amphiphilic nature the triblock copolymer Pluronics forms micelles in aqueous solutions to lower the free energy in a similar fashion as the non-ionic surfactants. As for the former surfactants, the concentration and temperature of the solution is crucial for the formation of micelles. On the other hand, micellization of Pluronic copolymers in water is

Fig. 9 O 1s XPS spectra for (A) Zn$_{Ac}$P0T90 and (B) Zn$_{Ac}$P10T90 samples prepared in the absence and presence of Pluronic P123, respectively.

Table 2 XPS relative composition of the O 1s peak for the series of ZnO samples prepared with increasing Pluronic concentration[a]

Sample	P123 concentration (n_{P123}/n_{Ac}) molar ratio	O_{LBE}* (at%)	O_{HBE}** (at%)
Zn$_{Ac}$P0T90	0.00	45	15
Zn$_{Ac}$P7T90	0.07	39	21
Zn$_{Ac}$P14T90	0.14	37	23
Zn$_{Ac}$P10T90	0.10	33	27

[a] Atomic percentage of low binding energy (*O_{LBE}) and high binding energy (**O_{HBE}) O 1s component for the various ZnO samples prepared with different amount of Pluronic P123.

very sensitive to the presence of additives. The interaction of urea (a salting-in compound) with various Pluronic copolymers is detailed in.[36] According to these authors, in the presence of urea the CMT (critical micelles temperature) of Pluronic copolymers is shifted to higher values.[36] These micelles consist of a hydrophobic polypropylene oxide core surrounded by hydrophilic polyethylene oxide chains that form a shell around the core. Therefore, polar urea molecules and Zn aquo-complex would interact with the terminal hydroxyl groups of the hydrophilic shell of P123 micelles. As the temperature increases, the urea hydrolysis begins leading to NH_4^+ and HCO_3^- ions that react with Zn^{2+} to form HZC nuclei. Because of this particular interaction, the precipitation and subsequent growth of HZC particles is expected to occur in these preferential sites near the micelles-urea interface, resulting in the oriented growth of ZnO crystals in the form well dispersed of micro-flowers. In the absence of Pluronic P123, the homogeneous nucleation of ZHC particles occurs and large spherical structures are formed during the growth process (Fig. 3A and 15E). The copolymer is then removed during washing and the obtained ZHC solid is then heated forming either well-dispersed ZnO microflowers (Zn_{Ac}P10T90, with P123) or larger crystals of ZnO in the absence of P123 (Zn_{Ac}P0T90).

Apart from the morphological differences, the polarity of ZnO products, ($I_{(002)}/I_{(100)}$), is also affected by the use of Pluronic P123. In fact, in the absence of Pluronic P123, the growth of ZnO crystals occurs mainly along the c-axis leading to the preferential exposure of nonpolar facets. On the contrary, in the Pluronic-assisted hydrothermal reaction, ZnO crystals are formed according to an oriented-growth process that preferentially occurs perpendicularly to the c-axis direction. As a result, more polar structures are obtained.

The growth habit of ZnO solids under hydrothermal conditions is well-documented in the literature.[33,37,38] The growth velocities under hydrothermal conditions along the different directions are known to follow the pattern $V(0001) > V(10\overline{1}1) > V(10\overline{1}0)$.[39] The relative growth rate of these crystal faces will determine the final shape and aspect ratio of the ZnO structures. In the absence of any external driving force, growth along the polar facets (c-axis direction) is favoured due to their high surface energy. As such, the preferred morphology of ZnO is hexagonal with crystals elongated along the c-axis, as for the sample prepared without Pluronic P123 herein. However, the crystal growth habit can be modified by selective adsorption of additives on the polar planes.[19]
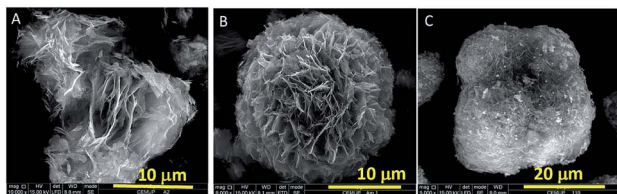
Under our experimental conditions, the preferential interaction of P123 micelles with the surface of metastable polar facets of ZnO lowers their surface energy, slowing down their growth. Because of this, the lateral growth of ZnO crystals (perpendicular to the c-axis) is stabilized leading to the formation of ZnO micro-flowers whose surface is dominated by polar facets. Similarly, in the absence of Pluronic P123 the ZHC particles formed during the nucleation step grow and evolve into large cluster in order to minimize the surface energy, as a consequence the growth occurs preferentially at expense of the polar planes (along the c-axis), which are less stable,[39] leading to the typical ZnO solids with preferential exposure of nonpolar facets.

The influence of the hydrothermal reaction temperature

The morphological evolution of the ZnO samples prepared at different reaction temperatures is illustrated in Fig. 10. The sample prepared at 70 °C (Zn_{Ac}P10T70, Fig. 10A) exhibits an irregular shape (quasi-flower-like structure) that resembles to an early stage of the flower-like morphology obtained at 90 °C (Zn_{Ac}P10T90); the latter is composed of assemblies of ZnO sheets (Fig. 10B). Further increase of reaction temperature up to 110 °C (Zn_{Ac}P10T110) resulted in the agglomeration of ZnO particles that appear assembled in the form of large cauliflower-like structures (Fig. 10C). On the other hand, it was found that the end pH of the hydrothermal reaction medium also increases with synthesis temperature; it increases from its initial value of 5.0 to 7.0, 8.4 and 9.1, when the reaction temperature was 70 °C, 90 °C and 110 °C, respectively. Hence, it is observed that the morphology of ZnO samples markedly changes with reaction temperature, in particular, the degree of compactness increases while increasing the temperature. Clearly the morphology strongly depends on the reaction temperature (and pH), which in turn controls the rate of urea decomposition.

The morphological changes observed in Fig. 10 are likely due to the temperature dependence of urea decomposition. Seeing

Fig. 10 SEM images of the ZnO samples synthesized at different hydrothermal temperatures: (A) 70 °C (Zn_{Ac}P10T70); (B) 90 °C (Zn_{Ac}P10T90) and (C) 110 °C (Zn_{Ac}P10T110).
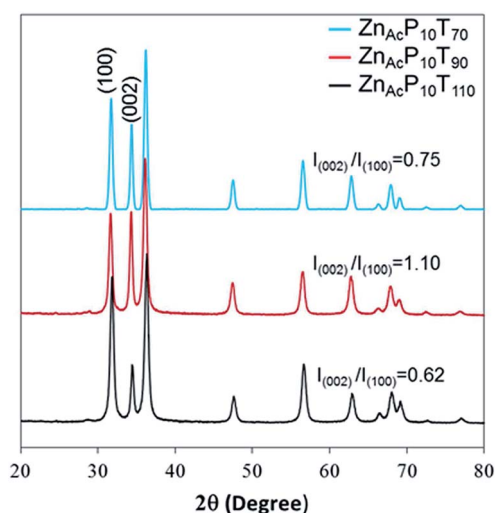

Fig. 11 XRD pattern and ($I_{(002)}/I_{(100)}$ ratio) of the ZnO samples prepared at different hydrothermal temperatures.

that the urea content was identical in the three experiments, the lower pH values encountered at lower reaction temperature suggest slow urea decomposition rates and *vice versa*. According to the literature, the urea decomposition is a temperature-dependent reaction that is favored at relatively high temperatures, typically above 90 °C.[40,41] At 70 °C (lower pH) the urea hydrolysis is slow, so that the concentration of ammonium and bicarbonate ions is low and consequently less ZnO particles are formed leading to the quasi-flower structures of Fig. 10A. However, at 90 °C the urea decomposition is faster and more ZnO particles are formed, giving rise to the micro-flowers in Fig. 10B. Finally, at 110 °C the urea hydrolysis is likely too fast which might cause the agglomeration and formation of the large cauliflower-like architectures shown in Fig. 10C.

The specific surface area of this group of samples increases with hydrothermal temperature in the 70–90 °C interval ($S_{BET} =$ 64 and 80 $m^2 g^{-1}$, for Zn_{Ac}P10T70 and Zn_{Ac}P10T90). Further increase of reaction temperature causes a significant decrease of the specific surface area (Zn_{Ac}P10T110 $S_{BET} = 50 \ m^2 g^{-1}$). The evolution of the S_{BET} with temperature is in good agreement with the formation of larger ZnO agglomerates at higher reaction temperature, as evidenced by SEM.

It was found that the peak intensity of XRD for the analyzed samples tends to increase with the temperature (Fig. 11). Since the sample weight used in XRD analysis is nearly the same, this is attributed to a higher degree of crystallinity of the resulting ZnOs. Regarding the polarity of this series of samples, it is observed that sample Zn_{Ac}P10T70 shows nearly the same value ($I_{(002)}/I_{(100)} = 0.75$) as the wurtzite ($I_{(002)}/I_{(100)} = 0.73$). This suggests that both samples follow the typical growth habit of wurtzite with preferential orientation along *c*-axis, resulting in ZnO materials whose surface is dominated by non-polar planes. The sample Zn_{Ac}P10T90 exhibits the highest polarity ($I_{(002)}/I_{(100)} = 1.10$), which represents a higher ratio of exposed polar facets, as already indicated. The Zn_{Ac}P10T110 sample has the lowest polarity among this series of samples, which is even lower than the wurtzite. This indicates that this sample has a higher ratio of non-polar planes. The variation in polarity observed here is probably related to the different morphology of the various samples. By comparison, the ZnO particles obtained at 90 °C show the optimal morphology, S_{BET} and also polarity.

Evaluation of the photocatalytic activity

The photocatalytic activity of a semiconductor such as ZnO depends on the optical properties, specific surface area, particle size and morphology of the particles.[13,42–44] In particular a high polarity (higher number of defects) and high specific surface area are expected to increase the photocatalytic activity of ZnO materials.[13,45]

The results presented in preceding sections evidence that both the polarity and specific surface area of ZnO materials prepared by the hydrothermal route depend on the synthesis conditions. To discriminate if the photoactivity of the prepared ZnO samples is influenced by the S_{BET} and/or the polarity, samples with similar S_{BET} but greatly differing in

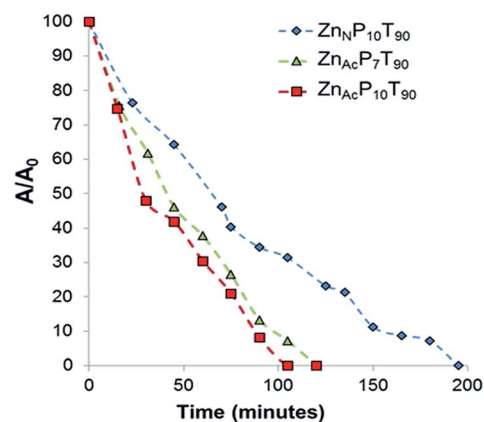Fig. 12 Photocatalytic degradation of MB over: Zn_{Ac}P10T90 ($S_{BET} = 80$ $m^2 g^{-1}$; $I_{(002)}/I_{(100)} = 1.10$), Zn_NP10T90 ($S_{BET} = 76 \ m^2 g^{-1}$; $I_{(002)}/I_{(100)} = 0.62$) and Zn_{Ac}P7T90 ($S_{BET} = 53 \ m^2 g^{-1}$; $I_{(002)}/I_{(100)} = 0.92$). Lines are for readability.

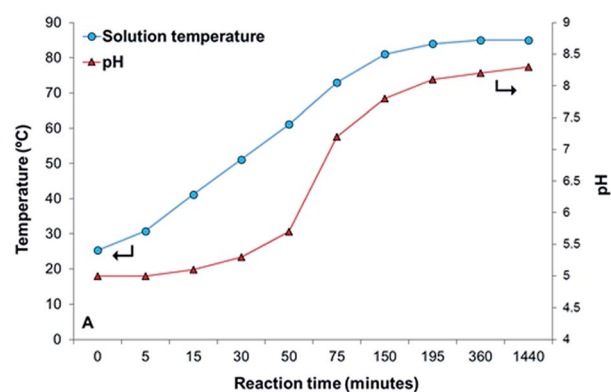Fig. 13 pH and temperature of the hydrothermal solution as a function of the reaction time for the Zn_{Ac}P10T90 sample. Lines are for readability.

polarity (Zn_{Ac}P10T90 and Zn_NP10T90) and samples with similar polarity but with very different specific surface areas (Zn_{Ac}P10T90 and Zn_{Ac}P7T90) were selected. The idea is to use the photocatalytic test as an indirect confirmation of polarity trends. Accordingly, the degradation of methylene blue (MB) was assessed using the three ZnO samples already mentioned: Zn_{Ac}P10T90, Zn_NP10T90 and Zn_{Ac}P7T90. Fig. 12 shows the results obtained. Sample Zn_NP10T90 (lowest polarity) exhibited a lower degradation rate, taking approximately 200 min to achieve total photocatalytic degradation. On the other hand, samples with higher polarity (Zn_{Ac}P10T90 and Zn_{Ac}P7T90) exhibited a prominent photocatalytic activity degrading the MB in 100–120 min, despite having different S_{BET} areas. These results show that the photoactivity of the prepared ZnO materials, under the present operating conditions, depends on the polarity rather than the S_{BET} surface area. On the other hand our "more polar" ZnO materials (Zn_{Ac}P10T90 and Zn_{Ac}P7T90) show comparable[46] or better[47,48] photocatalytic performance as compared to other ZnOs tested under similar operating conditions.

Role of Pluronic P123 on the ZnO formation mechanism

To gain some understanding about the role of the Pluronic P123 on the formation, growth process and morphology of HZC precursor two samples, with and without P123, were prepared following the same experimental protocol as that used for the synthesis of samples $Zn_{Ac}P10T90$ and $Zn_{Ac}P0T90$. During both syntheses a small amount of sample was taken out at different intervals and characterized by SEM-EDX. It should be noted that no product was collected if the hydrothermal time was inferior to 30 minutes (in the presence of P123) and 215 minutes (without P123). The evolution of the pH and temperature of hydrothermal solution during sampling was also recorded. The results are displayed in Fig. 13.

The temperature of the solution steadily increased during the first 3 h of reaction stabilizing at *ca.* 85 °C (Fig. 13) until the end of the synthesis (24 h). The variation of pH with reaction time follows a similar trend (Fig. 13); it slightly increases with temperature during the first 50 minutes of reaction, then it
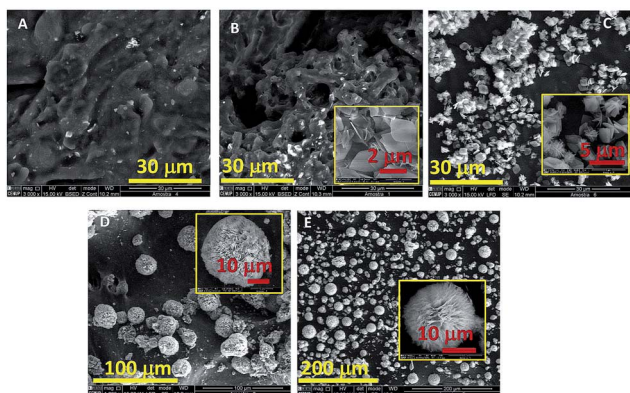

Fig. 14 SEM images showing the morphology evolution during the synthesis of the HZC in the presence of Pluronic P123 (same synthesis conditions as for $Zn_{Ac}P10T90$ sample: Zn-acetate, 0.10 (n_{P123}/n_{Ac}) molar ratio and 90 °C), after: (A) 30 min, (B) 75 min, (C) 150 min, (D) 195 min and (E) 24 h.
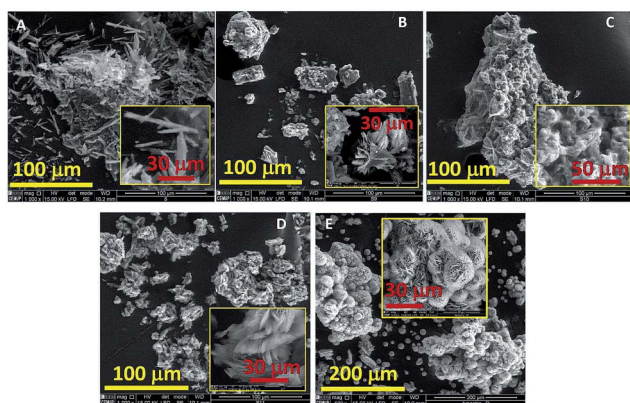

Fig. 15 SEM images showing the morphology evolution during the synthesis of the HZC in the absence of Pluronic (same synthesis conditions as for $Zn_{Ac}P0T90$ sample: Zn-acetate, no P123 and 90 °C), after: (A) 215 min, (B) 230 min, (C) 250 min, (D) 270 min and (E) 24 h.

increases sharply between 60 °C to 82 °C, and finally reaches a constant value of around 8.4. The pH history is essentially related to the homogeneous urea decomposition. Consequently, the formation and growth of HZC precipitate particles should be governed by the gradual urea hydrolysis, as nicely illustrated in Fig. 13.

The different contrast in the low voltage SEM images in Fig. 14A and B suggests some degree of heterogeneity in these samples. Accordingly, the EDX images of these materials show that in the bright areas Zn is the major element. The dark shades have a different composition, where N and C appear as the main components along with O and traces of Zn; urea should be the main component of these regions.

As mentioned, some Zn-rich particles (bright areas in Fig. 14A) are already formed during the first 30 minutes of the hydrothermal reaction. At this stage and according to Fig. 13, the urea hydrolysis is likely very slow due to the low temperature of hydrothermal solution, so the equilibrium of urea hydrolysis is shifted towards the left side, in good agreement with EDX results that indicate high N contents. This is also consistent with the low pH (Fig. 13), which evidences that the equilibrium of urea hydrolysis (eqn (2)) lies to the left side; there is a much greater concentration of urea than bicarbonate and ammonium ions, and no significant H^+ consumption take place, so pH remains essentially unchanged at 5. This also agrees with reported works on urea hydrolysis.[40] After 75 minutes of reaction, HZC species in the form of thin sheets are formed, as shown in the inset of Fig. 14B. As the reaction proceeds, the number of HZC particles increases (Fig. 14C), and the sheets appear now assembled in larger structures (inset in Fig. 14C). The spherical particles observed after 3 h of reaction (Fig. 14D) strongly resemble the micro-flowers observed after 24 h of hydrothermal reaction (inset in Fig. 3B).

Similar experiments were conducted in the absence of Pluronic P123. The obtained SEM images are shown in Fig. 15. In this case the precipitated particles are formed at much higher reaction times (215 min *vs.* 30 min in the synthesis without P123).

As apparent in this figure, the morphology evolution of the various materials with reaction time follows a similar tendency to that found in the presence of P123, although the solids show quite different morphology. In general, larger clusters are formed in the absence of Pluronic P123, as observed in Fig. 3A and 15E (final product). Interestingly, the SEM images of the resulting HZC material in Fig. 14E (after 24 h of reaction), shows that spherical clusters are formed regardless of Pluronic P123, but they appear better dispersed and have a more uniform aggregate size when P123 is used.

Thus, it is clear that under identical synthesis conditions, the use of Pluronic P123 enhances the dispersion of the formed HZC precipitates with the spherical morphology being characteristic of this kind of zinc basic hydroxy carbonates (ZHC).

In order to understand the role played by the Pluronic P123 on the formation process of ZnO in our experimental conditions, the aqueous chemistry of zinc and the urea hydrolysis will be analyzed henceforth.

Upon dissolution of a zinc salt in water, Zn^{2+} cations become octahedrally coordinated forming $[Zn(OH_2)_6]^{2+}$. The hexaqua zinc species are quite stable in very acidic medium but undergo hydrolysis at higher pHs. According to the literature[49,50] around pH 5 cations $[Zn(OH_2)_5(OH)]^+$ are the predominant species in solution. Thus, initial conditions of pH and temperature (at instant $t = 0$, in Fig. 13), urea and Pluronic P123 are stable in solution, since the solution temperature is very low (room temperature) for the urea decomposition and Pluronic micellization, and zinc is mostly as $[Zn(OH_2)_5(OH)]^+$. The mixture is then heated and the temperature of the solution gradually increases and around 50 °C micellization of Pluronic P123 is expected to occur.[36] The Pluronic micelles would interact with the polar species existing in solution, creating in this way the active sites for further nucleation and growth. At this point, the temperature is still too low for urea hydrolysis, and since the pH remains unchanged around 5, $[Zn(OH_2)_5(OH)]^+$ species are stable in solution. However, the solution temperature continues increasing and around 70 °C fast urea decomposition occurs. The optimum temperature for the urea hydrolysis is at about 85 °C,[40] which is accompanied by a sharp increase of pH (herein, after 75 minutes, Fig. 13). The decomposition of urea in aqueous solutions takes place in two stages.[40] The first one involves the formation of ammonium cyanate, which is followed by the irreversible hydrolysis of cyanate ions. Thus, the hydrolysis of urea can be written as follows:

$$CO(NH_2)_2 + 3H_2O \leftrightarrow HCO_3^- + 2NH_4^+ + OH^- \quad (2)$$
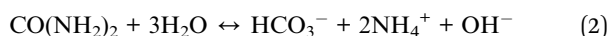
Obviously, the extent of the reaction defines the release of bicarbonate ions and OH^-, resulting in a gradual increase of pH, as observed in Fig. 13. According to,[50] $[Zn(OH_2)_5(OH)]^+$ species are complexed by HCO_3^- anions giving rise to $[Zn(OH)(HCO_3)(OH_2)_3]$. On the other hand, as pH raises the former species become unstable and undergo ligand exchange between the OH^- and HCO_3^- leading to neutral $[Zn(OH_2)_4(OH)_2]$ species.

Then, in the experimental conditions of the present study, the HZC nuclei are likely generated from condensation reactions between both $[Zn(OH_2)_4(OH)_2]$ and $[Zn(OH)(HCO_3)(OH_2)_3]$ according to eqn (3):[50]

$$3[Zn(OH_2)_4(OH)_2] + 2[Zn(OH)(HCO_3)(OH_2)_3] \rightarrow$$
$$Zn_5(OH)_6(CO_3)_2 + 20H_2O \quad (3)$$
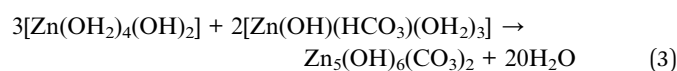
The formed nuclei then grew up to produce primary ZHC nanoparticles, which aggregated to form sheets (Fig. 14B). Subsequent growth leads to larger HZC structures (Fig. 14C and D), which are thermodynamically more stable, and finally to the hierarchical micro-flowers in Fig. 14E. In the synthesis carried out with Pluronic P123, since the nucleation process occurs in preferential sites, highly dispersed ZHC microflowers are generated from an oriented growth mechanism. However, in the absence of Pluronic, homogeneous nucleation takes place randomly, which leads to the formation of larger HZC particles during the growth step (Fig. 14) that undergo agglomeration giving rise to the large structures displayed in Fig. 14E. Finally,

the HZC solid will decompose into ZnO upon heating according to eqn (1), releasing CO_2 and H_2O (as evidenced by TPD and TG) to generate the porous ZnO microstructures illustrated in Fig. 4E. Moreover, the ZnO solid synthesized in the presence of P123, $Zn_{Ac}P10T90$ sample, after calcination maintains the original flower-like architectures as well as the highly dispersion as for the HZC precursor (Fig. 4E). As a result of the low dispersion, the sample obtained without P123 ($Zn_{Ac}P0T90$), leads to a more compact and shapeless ZnO material after calcination, as illustrated in Fig. 4C.

Comparing Fig. 14 and 15 it can be seen that the nucleation-growth process depends on the presence of P123. In this former case, P123 acts as a template, providing the sites for nucleation and growth, contributing to the formation of highly dispersed ZHC particles during growth. As a result homogeneous and dispersed ZnO solids in the form of microflowers are obtained upon calcination. Our results suggest that Pluronic P123 acts as growth director and dispersing agent.

Conclusions

Pluronic P123 block copolymer strongly influenced the morphology, polarity and specific surface area of the ZnO materials prepared by the urea-assisted hydrothermal method. In the presence of Pluronic P123, hierarchical ZnO microflowers whose surface is dominated by (002) polar planes were formed. Contrarily to this, large cluster agglomerates are formed in its absence and the surface is dominated by (100) non-polar planes. Moreover, the use of Pluronic P123 leads to ZnO materials with enhanced S_{BET}. The morphology and polarity is also affected by changing the metal salt from zinc acetate to zinc nitrate precursor. In this latter case, an urchin-like structure is obtained and the proportion of polar planes is only of 0.60 ($Zn_NP10T90$). The synthesis temperature seems to affect the decomposition rate of urea, being obtained at 70 °C and 110 °C quasi-flower and large cauliflower-like architectures, respectively. The materials with higher polarity showed higher photocatalytic activity for the decomposition of methylene blue, evidencing that even with similar surfaces areas the polar surfaces are more reactive, mainly due to the higher number of defects such as oxygen vacancies. The role of Pluronic P123 in the initial steps of the hydrothermal synthesis was clearly visible through backscattering images on SEM, acting as a template and providing the sites for nucleation and growth. This simple and easily scalable method allows the synthesis of ZnO with a highly faceted morphology, combined with high surface area and polarity, making these materials very promising for several applications such as catalysis.

Acknowledgements

Notes and references

1 S. Du, Y. Tian, H. Liu, J. Liu and Y. Chen, *J. Am. Ceram. Soc.*, 2006, **89**, 2440.

2 D. Polsongkram, P. Chamninok, S. Pukird, L. Chow, O. Lupan, G. Chai, H. Khallaf, S. Park and A. Schulte, *Phys. B*, 2008, **403**, 3713.

3 O. Lupan, L. Chow, G. Chai, B. Roldan, A. Naitabdi, A. Schulte and H. Heinrich, *Mater. Sci. Eng., B*, 2007, **145**, 57.

4 J. Bao, M. A. Zimmler and F. Capasso, *Nano Lett.*, 2006, **6**, 1719.

5 Th. Aeugle, H. Bialas, K. Heneka and W. Pleyer, *Thin Solid Films*, 1991, **201**, 293.

6 M. H. Huang, S. Mao, H. Feick, H. Yan, Y. Wu, H. Kind, E. Weber, R. Russo and P. Yang, *Science*, 2001, **292**, 1897.

7 L. Shen, N. Bao, K. Yanagisawa, K. Domen, C. A. Grimes and A. Gupta, *J. Phys. Chem. C*, 2007, **111**, 7280.

8 B. Meyer and D. Marx, *Phys. Rev. B: Condens. Matter Mater. Phys.*, 2004, **69**, 235420.

9 F. Ostendorf, S. Torbrügge and M. Reichling, *Phys. Rev. B: Condens. Matter Mater. Phys.*, 2008, **77**, 041405.

10 M. S. Spencer, *Top. Catal.*, 1999, **8**, 259.

11 H. Wilmer, M. Kurtz, K. V. Klementiev, O. P. Tkachenko, W. Grunert, O. Hinrichsen, A. Birkner, A. Rabe, K. Merz, M. Driess, C. Wo and M. Muhler, *Phys. Chem. Chem. Phys.*, 2003, **5**, 4736.

12 S. J. Kim and D. W. Park, *Appl. Surf. Sci.*, 2009, **255**, 5363.

13 R. Ullah and J. Dutta, *J. Hazard. Mater.*, 2008, **156**, 194.

14 O. Dulub, M. Batzill and U. Diebold, *Top. Catal.*, 2005, **36**, 65.

15 C. Wöll, *Prog. Surf. Sci.*, 2007, **82**, 55.

16 K. Dai, G. Zhu, Z. Liu, Q. Liu, Z. Chen and L. Lu, *Mater. Lett.*, 2012, **67**, 193.

17 G. K. Smith, S. Lin, W. Lai, A. Datye, D. Xie and H. Guo, *Surf. Sci.*, 2011, **605**, 750.

18 M. B. Boucher, S. Goergen, N. Yia and M. Flytzani-Stephanopoulos, *Phys. Chem. Chem. Phys.*, 2011, **13**, 2517.

19 G. R. Li, T. Hu, G. L. Pan, T. Y. Yan, X. P. Gao and H. Y. Zhu, *J. Phys. Chem. C*, 2008, **112**, 11859.

20 A. McLaren, T. Valdes-Solis, G. Li and S. C. Tsang, *J. Am. Chem. Soc.*, 2009, **131**, 12540.

21 J. Chang and E. R. Waclawik, *CrystEngComm*, 2012, **14**, 4041.

22 P. D. Burton, E. J. Peterson, T. J. Boyle and A. K. Datye, *Catal. Lett.*, 2010, **139**, 26.

23 S. Baruah and J. Dutta, *Sci. Technol. Adv. Mater.*, 2009, 10.

24 R. Pérez-Hernández, A. Gutiérrez-Martínez, A. Mayoral, F. L. Deepak, M. E. Fernández-García, G. Mondragón-Galicia, M. Miki and M. José-Yacamán, *Adv. Mater. Res.*, 2010, **132**, 205.

25 Q. Tang, W. Zhou, J. Shen, W. Zhang, L. Kong and Y. Qian, *Chem. Commun.*, 2004, **6**, 712.

26 M. Raula, M. H. Rashid, T. K. Paira, E. Dinda and T. K. Mandal, *Langmuir*, 2010, **26**, 8769.

27 F. Fang, N. Amc, X. Y. Chen, A. B. Djurišić and W. K. Chan, *AIP Conf. Proc.*, 2011, **1399**, 251.

28 M. Gusatti, G. S. Barroso, C. E. Maduro de Campos, D. A. Ribeiro de Souza, R. B. Lima, C. C. Milioli, L. A. Silva, H. G. Riella and N. C. Kuhnen, *Mater Res*, 2011, **14**, 264.

29 Z. L. Wang, *J. Phys.: Condens. Matter*, 2004, **16**, R829.

30 Y. K. Hsu, Y. G. Lin and Y. C. Chen, *Electrochem. Commun.*, 2011, **13**, 1383.

31 S. Xu and Z. Wang, *Nano Res.*, 2011, **4**, 1013.

32 P. Yang, H. Yan, S. Mao, R. Russo, J. Johnson, R. Saykally, N. Morris, J. Pham, R. He and H. J. Choi, *Adv. Funct. Mater.*, 2002, **12**, 323.

33 H. Zhang, D. Yang, X. Ma, Y. Ji, J. Xu and D. Que, *Nanotechnology*, 2004, **15**, 622.

34 P. Bai, P. Wu, Z. Yan, J. Zhou and X. S. Zhao, *J. Phys. Chem. C*, 2007, **111**, 9729.

35 Y. Peng, D. Huo and L. Zhu, *J. Phys.*, 2011, **263**, 012018.

36 J. H. Ma, C. Guo, Y. L. Tang, L. Chen, P. Bahadur and H. Z. Liu, *J. Phys. Chem. B*, 2007, **111**, 5155.

37 L. Shi, A. J. T. Naik, J. B. M. Goodall, C. Tighe, R. Gruar, R. Binions, I. Parkin and J. Darr, *Langmuir*, 2013, **29**, 10603.

38 H. Zhang, D. Yang, X. Ma, Y. Ji, J. Xu and D. Que, *J. Phys. Chem. B*, 2004, **108**, 3955.

39 Z. Zhang and J. Mu, *J. Colloid Interface Sci.*, 2007, **307**, 79.

40 G. J. D. A. A. Soler-Iltia, M. Jobbagy, R. J. Candal, A. E. Regazzoni and M. A. Blesa, *J. Dispersion Sci. Technol.*, 1998, **19**, 207.

41 M. L. Kieke, J. W. Schoppelrei and T. B. Brill, *J. Phys. Chem.*, 1996, **100**, 7455.

42 L. Zhou, W. Wang, L. Zhang, H. Xu and W. Zhu, *J. Phys. Chem. C*, 2007, **111**, 13659.

43 L. Zhang, W. Wang, L. Zhou and H. Xu, *Small*, 2007, **3**, 1618.

44 L. Zhang, W. Wang, Z. Chen, L. Zhou, H. Xu and W. Zhu, *J. Mater. Chem.*, 2007, **17**, 2526.

45 A. Moulahi and F. Sediri, *Mater. Res. Bull.*, 2013, **48**, 3723.

46 Q. I. Rahman, M. Ahmad, S. K. Misra and M. B. Lohani, *Superlattices Microstruct.*, 2013, **64**, 495.

47 H. Usui, *J. Colloid Interface Sci.*, 2009, **336**, 667.

48 T. Sun, J. Qiu and C. Liang, *J. Phys. Chem. C*, 2008, **112**, 715.

49 D. Kisailus, B. Schwenzer, J. Gomm, J. C. Weaver and D. E. Morse, *J. Am. Chem. Soc.*, 2006, **128**, 10276.

50 M. Bitenc, P. Podbrscek, P. Dubcek, S. Bernstorff, G. Drazic, B. Orel, S. Pejovnik and Z. C. Orel, *Chem.–Eur. J.*, 2010, **16**, 11481.